Acta Astronautica 238 (2026) 103–111

Contents lists available at ScienceDirect

Acta Astronautica

journal homepage: www.elsevier.com/locate/actaastro

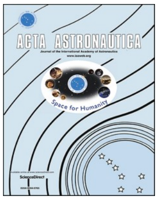

Rapid prototyping of satellite shields: 3D printed carbon fiber and Kevlar composites for hypervelocity impact protection

Stefano Lopresti [a,*], Leonardo Barilaro [b], Alberto Abiti [a], Lorenzo Olivieri [c]

[a] CISAS "G. Colombo", University of Padova, Via Venezia 1, 35131, Padova, PD, Italy
[b] Department of Aviation, The Malta College of Arts, Science & Technology, Triq Kordin, Paola, PLA 9032, Malta
[c] DII/CISAS, University of Padova, Via Venezia 1, 35131, Padova, PD, Italy

ABSTRACT

This study explores the potential of 3D-printed composite shields for protecting satellites against hypervelocity impacts from space debris. Using a novel approach that integrates carbon fiber and Kevlar filaments, the paper presents a cost-effective and time-efficient methodology development for rapid prototyping satellite protection systems. Ten test samples were designed and manufactured implementing a dual-filament 3D printing process, employing carbon fiber as the primary structural material and Kevlar as the core. These shields were tested under simulated orbital collision conditions using a two-stage light-gas gun. The experimental results demonstrate the shields' effectiveness against hypervelocity impacts, revealing a significant correlation between manufacturing parameters and impact resistance. Preliminary results suggest that this methodology enables the development of customized, efficient shielding solutions with reduced production times and costs. A follow-up experimental campaign is outlined to further refine the technology, optimize the associated uncertainty range and assess its broader applications in space systems. This research contributes to the growing field of space debris mitigation, offering a promising approach to enhancing the resilience of orbital assets against collision threats.

1. Introduction

The aerospace sector is undergoing a significant transformation, marked by the rapid growth of the small satellite market and the reduced launch costs democratizing the access to space [1]. This evolution is boosting the adoption of innovative technologies from terrestrial industries, that previously were only moderately adapted for space applications. Among these, additive manufacturing, or 3D printing, is emerging as a revolutionary tool for designing and producing satellite components. Its capacity to create complex geometries, optimize material properties, and drastically cut prototyping time and costs makes it uniquely suited to the demands of the modern space industry [2,3]. In particular, additive manufacturing allows the design and implementation of novel and high-performance solutions, that can be easily adapted to different mission profiles and requirements [4–6].

In parallel, the current proliferation of orbital debris poses an escalating and critical threat to the sustainability of space operations. With more than 50,000 pieces of debris being tracked and catalogued in Earth orbits and more undetected, the risk of hypervelocity impacts (HVIs) on active satellites and crewed spacecraft is rising [7]. This threat creates a dual challenge. First, there is the clear need to equip new satellites with increasingly efficient shields without affecting the spacecraft mass budget (and, consequently, the launch cost). Second, it is necessary to develop a viable strategy to repair damages sustained by long-duration missions, such as orbital stations like the ISS. Traditionally, repairing a damaged shield is a logistically complex and expensive operation, often necessitating the transport of large replacement panels and high-risk EVAs (Extravehicular activities).

One of the most promising applications is the development of 3D-printed repair patches for aerospace structures damaged by high-energy impacts [8,9]. The ability to produce such elements directly in orbit could revolutionize maintenance, repair, and overhaul (MRO) procedures for space assets, significantly reducing costs and risks. In particular, this study proposes a novel methodology to accelerate the development of such systems, integrating advanced simulation techniques with practical, cost-effective rapid prototyping. These innovations can enhance the effectiveness of protective systems while minimizing weight and volume, addressing critical challenges in space engineering [10,11].

The remainder of this paper presents a preliminary experimental campaign focused on 3D-printed shields composed of a carbon fiber structure and a Kevlar core. Ten samples were tested under simulated orbital collision conditions to assess the correlation between manufacturing parameters and impact resistance. The results propose a new, streamlined development pathway for customized shielding

---

* Corresponding author.
E-mail addresses: stefano.lopresti@phd.unipd.it (S. Lopresti), leonardo.barilaro@mcast.edu.mt (L. Barilaro), alberto.abiti@unipd.it (A. Abiti), lorenzo.olivieri@unipd.it (L. Olivieri).

https://doi.org/10.1016/j.actaastro.2025.08.029
Received 2 July 2025; Received in revised form 5 August 2025; Accepted 14 August 2025

Nomenclature

HVI	Hypervelocity Impact
EVA	Extravehicular activity
MRO	Maintenance, Repair, and Overhaul
MMOD	Micrometeoroids and Orbital Debris
FFF	Fused Filament Fabrication
CFRP	Carbon Fiber Reinforced Polymer
SPH	Smoothed-Particle Hydrodynamics
TRL:	Technology Readiness Level
DPI	Dots Per Inch
V_{res}	Residual velocity of the debris cloud
V_{Rad}	Radial velocity of the debris cloud
D_c	Debris Cloud Diameter
Beta	Debris Cloud angle with respect to the plate
I_c	Debris Cloud horizontal extension
V_x	Mean x velocity of the fragments
V_y	Mean y velocity of the fragments
t_d	Time at which a fragment is detected for the first time

solutions, aiming to prove the concept and pave the way for a new generation of more efficient and sustainable protection for orbital spacecraft.

2. State of the art

Rapid prototyping is crucial in satellite development for accelerating innovation and reducing costs by enabling early identification of design flaws [12]. By iterating through designs quickly, engineers can validate new technologies and refine objectives before committing to full-scale production. This is particularly valuable for the growing number of universities, startups, and research teams entering the space sector.

A promising field for the application of this methodology is the development of protective shields against micrometeoroids and orbital debris (MMOD. One of the bigger limitation of the current shields is the loss of protection capabilities after the collision with a MMOD in the entire region of the impact, and repair requires the complex and costly replacement of an entire panel, often involving an EVA. Additive manufacturing presents a transformative solution by enabling the possibility of printing repair patches directly in orbit) [13]. These patches could be customized to the exact size of the damage, optimizing material usage and restoring the original structural integrity of the spacecraft [14].

The aerospace industry was an early adopter of 3D printing, primarily for prototyping [15]. Today, its use has expanded to include end-use parts, driven by advancements in printing flame-retardant and high-strength composite materials. Fused Filament Fabrication (FFF) is a popular method that has evolved to incorporate reinforcements like carbon fiber to enhance the mechanical properties of thermoplastics like ABS, PEEK, and Nylon [16]. Generally, for these applications the approach is to use short, chopped fiber filament immersed in an epoxy matrix, although for high-performance applications, some continuous fiber structures have recently begun to be printed between the layers to better distribute loads and increase mechanical properties. The performance of FFF parts is highly dependent on process variables like raster angle, which can induce orthotropic behavior, and achieving strong interlayer bonding to minimize voids.

Previous research, such as the H2020 ReDSHIFT project [17], has already demonstrated that 3D-printed aluminum shields can be a valid alternative to traditionally manufactured ones, showing comparable ballistic properties. This study builds on the foundation of the Smart Ballistic Optimization for Repairing of Aerospace Exostructures using 3D printed Kevlar (SBORAEK) project, which developed ballistic-optimized, 3D-printed, continuous-fiber shields for high-energy impact applications in aerospace [18].

3. Methodology

This study provides a methodology for the rapid development and prototyping of satellite shields and reparative patches using 3D-printed carbon fiber reinforced polymer (CFRP) and Kevlar filaments.

The primary goal is to create and test a shield with a comparable mass to a traditional shield to evaluate its impact survivability in a hypervelocity facility.

3.1. Step by step development

The development process was designed to be rapid, accessible, and iterative, ensuring the methodology is affordable and simple to implement in any laboratory with (relatively) commonly available 3D printers and materials. The process follows these key phases.

- A preliminary step was a review study of existing literature on canonical carbon fiber shields to establish baseline parameters for thickness, manufacturing techniques, and previous test conditions. This was done to ensure the newly designed samples would be directly comparable to existing solutions.
- An initial design phase was conducted using a multi-objective optimization procedure to evaluate different geometries, masses, and expected failure thresholds. This was supported by coarse numerical simulations using an SPH algorithm to identify thicknesses expected to provide a ballistic response comparable to classical shields. This “simulation-first” approach is intended to shorten development time by reducing the need for extensive and costly ground experiments.
- Based on the simulation results, test samples were developed and manufactured. The focus was on creating fully functional and representative prototypes to achieve a proof-of-concept at Technology Readiness Level (TRL) 5.
- The prototypes were subjected to a preliminary hypervelocity test campaign to assess their performance under relevant conditions and validate the simulation models. Following the iterative approach of this methodology, once consolidated with accessible materials, a second development phase using more specialized materials and machinery can be undertaken. The data from the first test campaign is intended to refine the simulation models, creating a more accurate “digital twin” that can predict the performance of future designs and reduce the number of required physical tests.

The flowchart of the methodology is resumed in Fig. 1. Following this philosophy that reflects the principles of the concurrent engineering, it was possible to pass from the designing phase to the test in a reduced time, anticipating the problems and minimizing the costs.

3.2. Shields design

The shield design process is fundamentally driven by a hybrid simulation approach that combines empiric modeling with faster, scenario-based virtual testing.

The shields were produced with an Ultimaker S5 printer, chosen for its dual-nozzle capability, which is essential for printing with two different materials like carbon fiber and Kevlar that have different temperature and nozzle requirements (Fig. 2). The printer’s controlled environment and filament preservation system ensure precision and repeatability, even for samples printed weeks apart.

In Table 1 the selected printing parameters are reported.

For the samples, the DoE matrix was designed to test the combination of two different materials: for the structure it was selected a polyamide matrix reinforced with short carbon fibers embedded in omnidirectional orientation. In particular the printing was performed with the “Luvocom

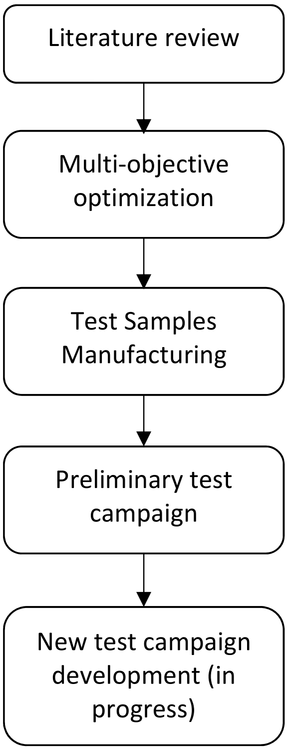

Fig. 1. Flowchart of the methodology

Path CF 9891 BK". For the core, instead, a Kevlar filament embedded in an ABS matrix manufactured by Kimya was chosen. The "Luvocom Path CF 9891 BK" has mechanical properties that are much lower than those of a carbon fiber panel, as the tensile strength is around 120 MPa and the modulus of elasticity is 120 GPa. Stiffness, however, is not the main property searched, and these parameters, combined with shock absorbing capabilities of Kevlar and ABS core, make it possible to have a panel that is rigid enough to be structural but capable of effectively dispersing the energy of an impacting projectile.

The samples produced are 150 mm squares with holes for hanging in the laboratory test chamber. The Kevlar layer is only placed in the center of the test specimen, in a square of side 70 mm (Fig. 3).

The nominal point of impact is the exact center of the sample, with the diameter of the impact tolerance area of 25 mm. The total thickness of the target is 12 mm, the thickness of the inner core is 6 mm. In order to reduce weight, the shields were printed at low density, as shown in Table 2.

For the test campaign, two sets of test samples were produced, a single-plate and a multi-plate structure, consisting of three single plates spaced 12 mm apart (Fig. 4).

In order to investigate also the influence of the printing direction on the ballistic capabilities of the test samples, the plates were manufactured following two different printing orientations: the orientation will be called "horizontal" if the plates are produced with the major face facing the printing plate, will be called "vertical" if a plate is printed with one of the thin faces facing the printing plate. In this test campaign, all the single plates, except for the one used for the test shot, were printed horizontally, while all multiplate were produced vertically.

4. Test campaign

The test campaign consisted of 10 tests, plus a centering test. The first five tests and the centering shot were performed on single plates, using a 3 mm-diameter aluminum ball as a projectile with a velocity varying from 3 to 5 a km/s. Tests 6 to 10, on the other hand, were performed on multiplate, using both aluminum and steel balls, at the same velocities.

The tests were performed with the 2-stage light gas gun "Hermes" in Thiot Ingegnerie's Shock Physics Lab (Fig. 5). For the recording, a high-speed Phantom V2012 camera was placed at the side of the target to capture images of the impact. Projectile speed is measured through the "VMS2000", a system based on four optical fibers that allows velocity to be measured by occlusion of laser beams with a measurement error of less than 1 %.

Behind each sample, at a distance of 100 mm, a soft ballistic gel catcher was placed to stop the fragments and collect some additional data on the debris cloud. All soft catchers were sent to the Malta College of Arts, Science, and Tecnology (MCAST) after the test campaign and analyzed. An example of the catcher is shown in Fig. 6; results regarding the generated fragments are still under evaluation.

Table 1
Printing parameters.

Process parameters	CFRP	Kevlar
Nozzle Diameter [mm]	0.8	0.4
Layer height [mm]	0.4	0.2
Print Speed [mm/s]	50	25
Print Temperature [C°]	280	260
Build plate temperature [C°]	65	//
Infill density [%]	Refer to Table 2	Refer to Table 2
Infill pattern	zig-zag	zig-zag
Built plate adhesion type	Brim	//

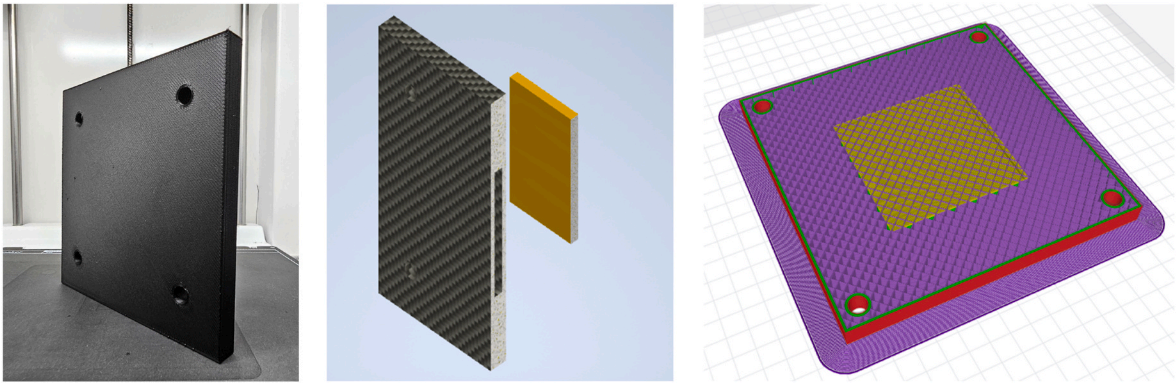

Fig. 2. 3D-printed samples layout: On the left: Printed test sample. In the center: composition of the samples. The outer CFRP shell is shown in black, while the Kevlar core is shown in yellow. On the right: the path of the nozzle during printing. (For interpretation of the references to colour in this figure legend, the reader is referred to the Web version of this article.)

Table 2
3D-printed samples test matrix summary.

Plate	Infill CFRP [%]	Infill Kevlar [%]	Configuration	Print direction	Impact Velocity [m/s]	Projectile material
0A (test)	8	20	Single wall	Vertical	4200.0	Aluminum
1	20	20	Single wall	Horizontal	2699.8	Aluminum
2	10	20	Single wall	Horizontal	4157.7	Aluminum
3	10	20	Single wall	Horizontal	4181.0	Aluminum
4	10	20	Single wall	Horizontal	4332.0	Aluminum
5	10	20	Single wall	Horizontal	5121.0	Aluminum
6	8	20	Multiple wall	Vertical	2755.4	Aluminum
7	10	20	Multiple wall	Vertical	4073.0	Aluminum
8	10	20	Multiple wall	Vertical	4920.7	Aluminum
9	10	20	Multiple wall	Vertical	5031.6	Steel
10	10	20	Multiple wall	Vertical	5250.8	Steel

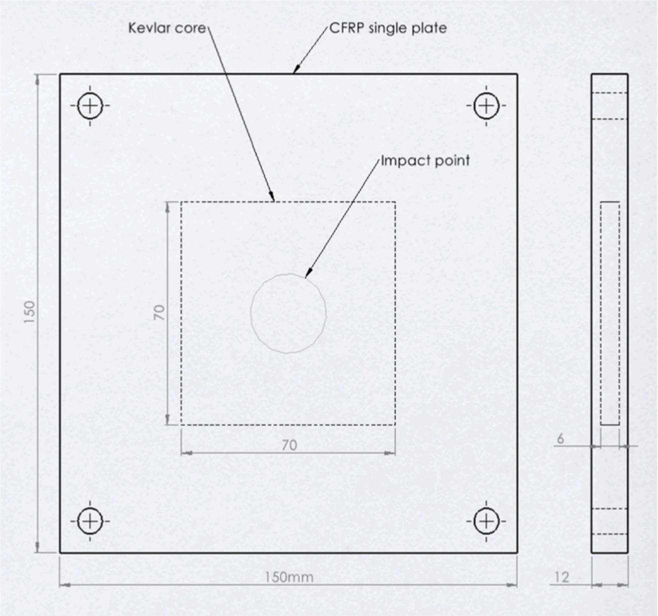

Fig. 3. 3D-printed sample dimensions.

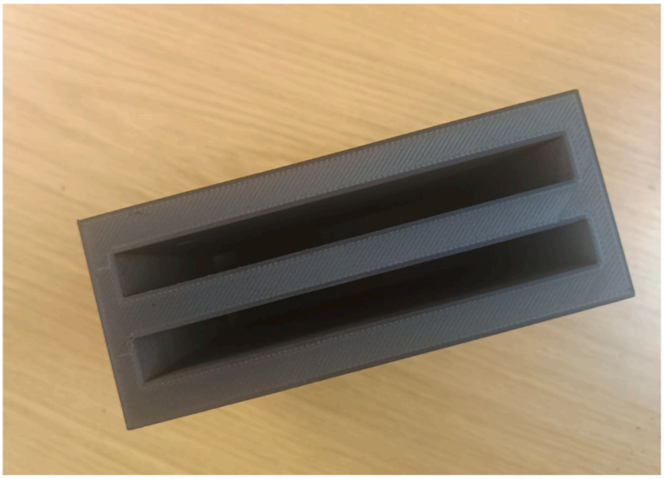

Fig. 4. Top view of the multiplate structures.

5. Test results

For each test, a projectile and sample weight measurement were taken before the test, and all samples were also weighed after the test. A photo of a plate after a test is shown in Fig. 7.

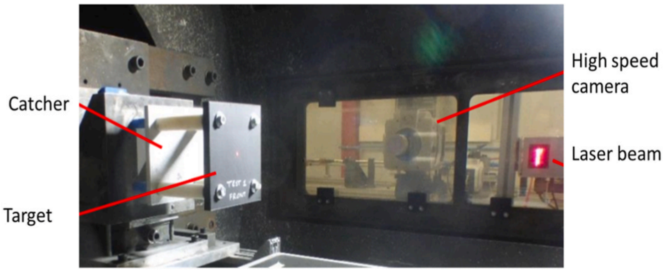

Fig. 5. Experimental setup. (Image courtesy of Thiot Ingegnerie).

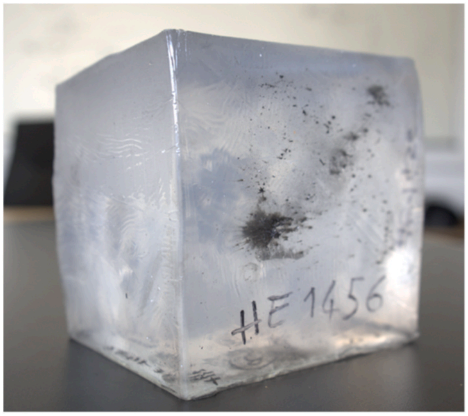

Fig. 6. Soft ballistic gel catcher placed behind the target.

All plates were then scanned from both sides using a 600 DPI scanner and the images were analyzed using a Matlab™ procedure that calculates the hole area. This step is particularly delicate as the damage on structures of this composition is not circular as is usually the case with isotropic materials but has a more irregular shape. The code then associates an ellipse (red) with the hole to best describe its edges; the value shown in the following tables is the arithmetic mean between the two semi-axes. In addition, the code is able to detect the area in which the entire CFRP layer has been damaged, exposing the inner Kevlar layer (blue). Finally, in yellow is identified the total area in which there was a surface delamination of the first layer as a result of the impact (Fig. 8).

The damage sustained by the 3D-printed shields, as measured using the described procedure, was compared across all the performed tests using an energetic parameter as the kinetic energy of the projectile. The following graph shows the crater size versus the kinetic energy of the impacting body (Fig. 9).

This first campaign doesn't aim to have a sufficient number of tests to make relevant statistics, but to identify some trends to be studied through future dedicated campaigns; furthermore, given the scarcity of experimental data on such materials, the authors emphasize the

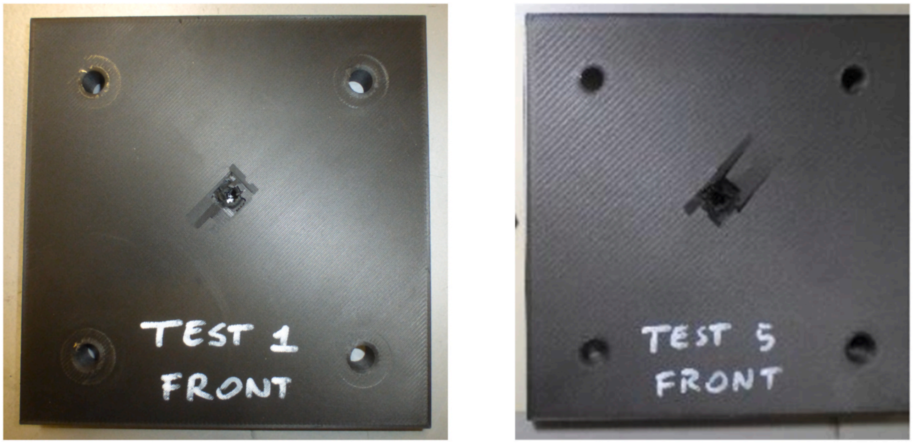

Fig. 7. Test 1 and Test 5 after impact. For the samples printed “horizontally” damage is localized and delamination of the first layers has been detected.

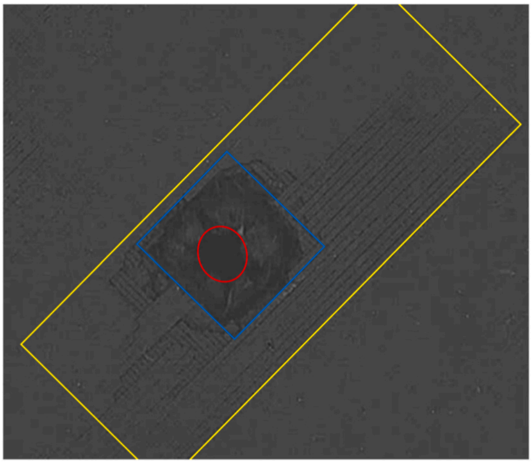

Fig. 8. Graphic representation of the damaged area identifying the crater (red), the inner damage (blue) and the total delamination (yellow). (For interpretation of the references to colour in this figure legend, the reader is referred to the Web version of this article.)

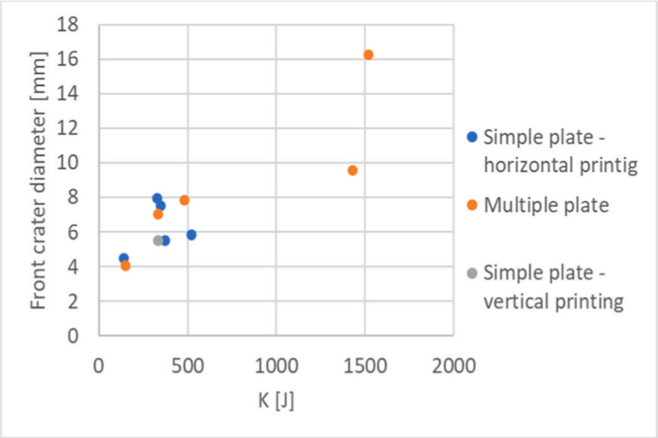

Fig. 9. Front crater diameter in function of impactor kinetic energy.

importance of disseminating these data in the scientific literature.

In this case it is possible to observe a clear tendency for multiplate, while the distribution of impacts on single plates is more chaotic. This discrepancy is due to the different printing direction of the plates. As the filling is between 10 % and 20 % and the internal structure of the plate is reticular, the ability of the projectile to penetrate and the damage done depends on the impact position on the underlying reticle, this leads to an uncontrollable degree of freedom that make extremely complex to describe the curve’s behavior mathematically. The situation changes when it comes to multiplate, since the velocity of motion is perpendicular to the direction of filling, the projectile encounters a material with more constant properties regardless of the actual point of impact.

With respect to surface delamination, however, the results seem to indicate that two different mechanisms drive in phenomena (Fig. 10).

For single-plate structures, the entire surface is made of a single printing layer, which remains more cohesive and even as the impact energy increases, does not delaminate excessively. In vertically-printed structures, on the other hand, the projectile strikes several layers laterally, which offer less resistance and, in the case of high-energy impacts, can result in a fracture between the layers that can be several millimeters deep (Fig. 11).

This is confirmed by the fact that the experimental point obtained with the test single plate, produced in the direction of the multiplate, aligns perfectly with the experimental points of the multiplate.

5.1. *Cloud analysis*

In addition, during the tests videos of the fragmentation were recorded using a Phantom v2012 ultrahigh-speed digital camera. In order to extract more information about the produced fragments and their time evolution, a video analysis of the produced debris cloud was performed using a Matlab™ code. As the first step, the code extracts the

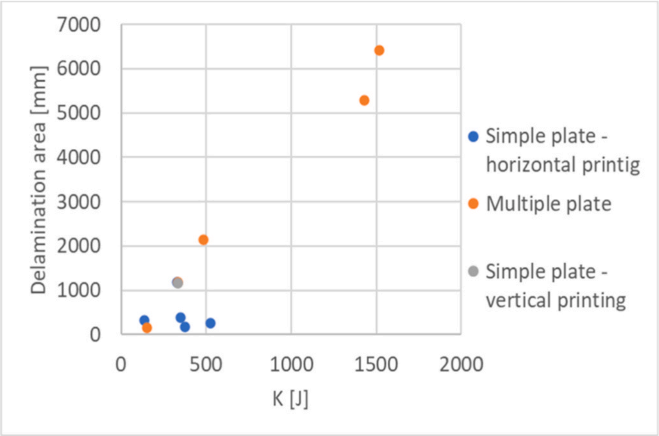

Fig. 10. Total delamination area in function of impactor kinetic energy.

Fig. 11. Test 7 and Test 8 after impact. For the samples printed “vertically” a crack is triggered and propagates between the layers of printed material.

frames of the video showing the first moments of the cloud propagation. For each frame of interest, after binarizing the image and selecting manually the area including only the cloud, it automatically measures the horizontal (blue) and vertical (green) limits of the cloud, as shown in Fig. 12.

At this point, it is possible to calculate the residual velocity of the cloud (V_{RES}), the radial velocity (V_{RAD}) and the values of the cloud diameter (d_C) and the angle (β), both measured at a specified value of the horizontal extension l_C. Results are summarized in Table 3. The measurements were possible only for single plates tests due to the insufficient number of frames showing the debris cloud before the impact with the rear wall of the multiple plate shields.

In contrast with the hole diameter in the front face, the evolution of the cloud appears to be very regular and the influence of the impact position seems absent. Below is the graph showing the coordinates of the longitudinal dimension and circumferential development of the cloud for the available frames. Interestingly, the points tend to align on the same curve (Fig. 13).

Plotting the radial and residual velocities of the normalized clouds against the initial velocities, it can be noted that these tend to respect constant ratios (Fig. 14).

Furthermore, Fig. 15 shows the value of $d_{C,}$ measured for $l_C = 11.61 \pm 2.00$ *mm*. The uncertainty of this value depends on the number of frames where the cloud extension was measurable. The plot suggests that in all tests, with the exception of test 3, d_C appears to have no significant variation over the uncertainty range, more data will be needed to confirm this hypothesis.

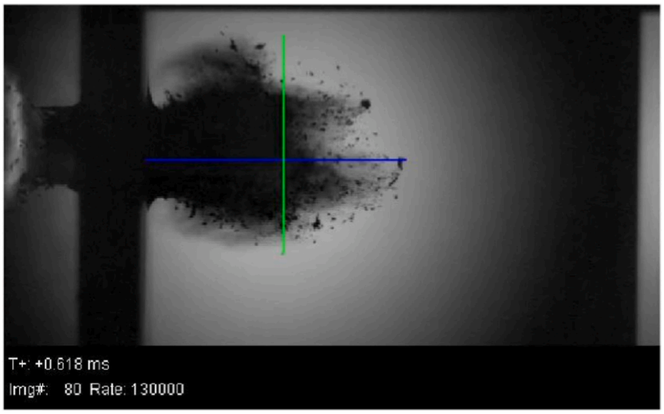

Fig. 12. Cloud extension analysis for plate 2 fragmentation video.

Table 3
Residual and radial velocities of the fragment clouds for single plate tests.

Plate	V_{RES} (m/s)	V_{RAD} (m/s)
0A	562.3	139.1
1	687.6	273.5
2	1470.1	889.1
3	1350.3	784.9
4	2015.1	1360.9
5	1257.8	278.1

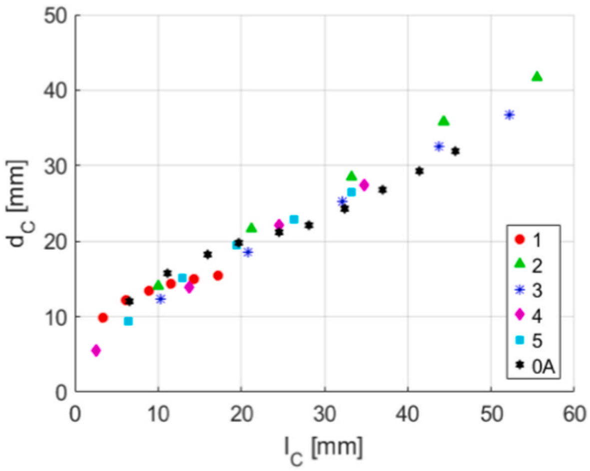

Fig. 13. Cloud diameter extension as a function of the cloud horizontal extension.
Different markers indicate the different simple plate tests.

5.2. *Fragments velocity analysis*

A further study was done by applying a Matlab™ procedure to the frames of the video to track the fragments and calculate their speed, instant by instant. The procedure can be divided into two main steps: the first part detects for each frame the center of mass and the area of the fragments as follows.

- The frame is converted to grayscale;
- The frame is binarized using an adaptive threshold;
- Adjacent pixels of the same type are connected to identify the fragment areas and their corresponding centers of mass.

The second part identifies the fragment trajectories. Starting from

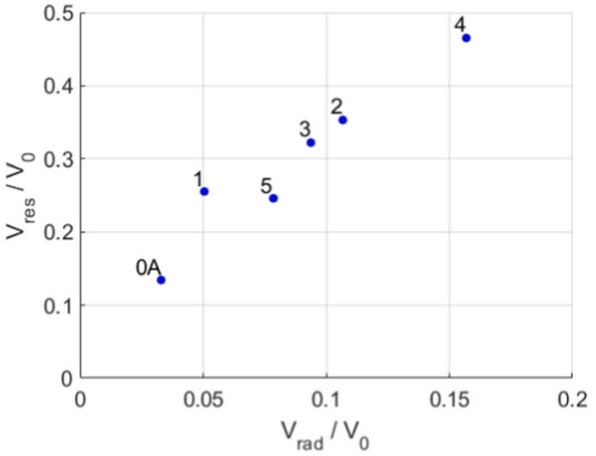

Fig. 14. Ratio between VRES and the impact velocity V_0 as a function of the ratio between V_{RAD} and V_0.

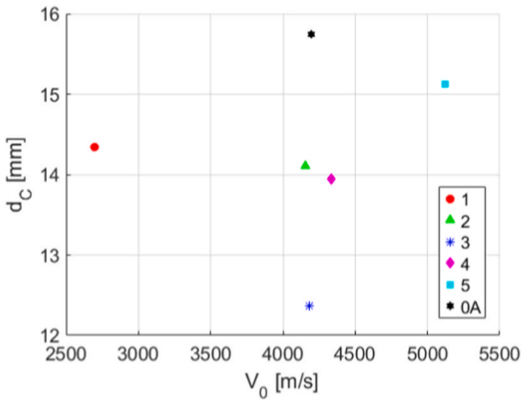

Fig. 15. d_C measured for $l_C = 11.71 \pm 2.00$ mm as a function of V_0.

the assumption that during the rapid evolution of the collision, the gravity effect on the fragments is negligible, the trajectories are considered to be straight lines. For this reason, a Random Sample Consensus (RANSAC) algorithm is applied to interpolate the detected centers of mass obtaining the straight trajectories. By overlaying the identified trajectories onto the video frames, the validity of this assumption can be confirmed.

From this procedure, it was possible to calculate various cinematic parameters of the fragments, such as their mean velocities in horizontal (V_X) and vertical (V_Y) direction. Fig. 16 presents a graph in which the time at which a fragment is detected for the first time (t_D) is shown in the abscissa and V_X is shown in the ordinate. t_D is assumed to be close enough to the time the fragment detached from the 3d printed plate. Fragment detection could be performed only for single plate tests, since multiplate tests showed no complete perforation or, as in test 10, there were not enough frames to complete the tracking.

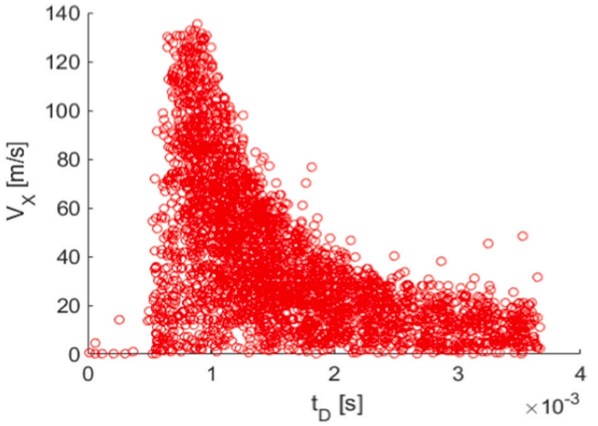

Fig. 16. Fragments velocities in horizontal direction as a function of the time of the first frame in which they become visible for test 2.

It can be observed that the detected fragment velocities uniformly populate a graph area outlined by a power-type curve, following equation (1)

$$V_X = A * t_D^B \tag{1}$$

The coefficients were determined through a non-linear fit and their values are reported in Table 4.

Finally, the curves, normalized by the initial velocity of the debris cloud V_{RES}, are represented in Fig. 17. However, it must be noted that during the initial moments of the collision, capturing individual fragments is particularly challenging as the cloud appears as a single body. For these moments, the curves are approximated using the equations while the fragments velocities remain lower than the cloud velocity V_{RES} shown in Table 2, and assuming a uniform velocity equal to V_{RES} when V_X exceeds that value.

The subtended area, normalized by the initial velocity of the impactor, can suggest information about the absorption capacity of each plate. In particular, test 0A exhibits a higher curve compared to the others, indicating that vertically printed plates absorb less energy than the horizontal printed plates.

5.3. *Uncertainties and error propagation in the analysis*

To properly contextualize the experimental results presented, an analysis of the uncertainty and error propagation within the measurement chain was conducted. The final uncertainty provides a confidence range for the data and establishes a benchmark for the comparison of future test results.

The primary sources of uncertainty were identified as.

1) Manufacturing tolerance: The 3D printer's nozzle size introduces a thickness uncertainty of ±0.8 mm, which is in line with tolerances for samples commonly produced in CFRP and was not considered a variable in this analysis. However, this tolerance contributes to the variability of the physical phenomenon rather than the measurement uncertainty, and it has been considered when evaluating the scatter in the final results
2) Projectile velocity: The light-gas gun's velocity measurement system has a declared sensitivity of ±1 %
3) Mass measurement: The uncertainty on mass measurements is 0.01g, which translates to a negligible relative uncertainty of approximately 0.01 % for the single plates.
4) Video analysis calibration: The largest source of error comes from the video analysis, specifically the calibration of the pixel size. This was calibrated by measuring the known size of the plate in a frame and calculating the pixel-to-mm ratio. However, varying the binarization threshold for this measurement resulted in a slight variation in the

Table 4
Summary table of coefficients used.

Test	A	B
0A	0.1886	−0.8184
1	0.0386	−0.9889
2	0.4547	−0.7175
3	0.2408	−0.8066
4	0.3263	−0.7023
5	0.2332	−0.7621

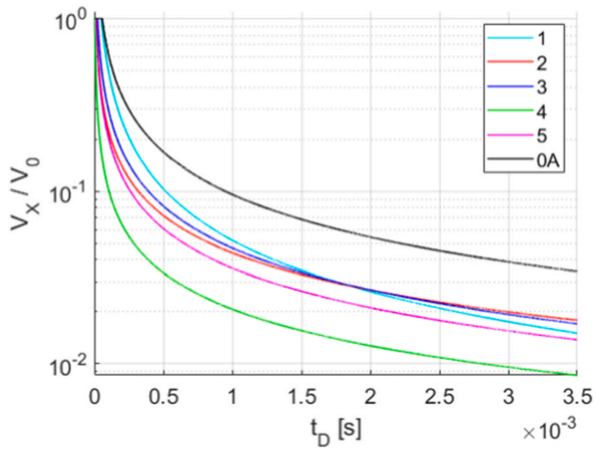

Fig. 17. Representation of the curves outlining the fragment horizontal velocity distributions, normalized by the collision speed, as a function of the time of the first frame in which they become visible.

calculated plate size, leading to a relative error of 5 % in the pixel dimensioning.

The total propagated uncertainty for parameters involving kinetic energy (E_k) and video analysis was calculated by combining the constituent errors.

Using kinetic energies, and thus multiplying the mass by the velocity squared, a conservative estimation of the error is derived from (2):

$$Err_{Ek} = 1 + 1 + 0,1 = 2,01\% \quad (2)$$

In video analysis, the uncertainty of the measurement is related to the uncertainty of the pixel size. This procedure was followed for calibration: a frame in which only the plate is visible was selected and was binarized according to a threshold, so as to have an image with white pixels for the background and black pixels for the plate, for each row the number of black pixels was counted, a mathematical average of the number of rows was made to have an average size of the width.

The actual size of the plate was then measured with a caliper and from the ratio of the measurements obtained, the pixel size was identified.

The uncertainty in this measurement is caused by the fact that depending on the threshold value selected, the average plate size calculated by the software may vary slightly. A relative error of 5 % is obtained from the ratio of the calculated maximum and minimum plate dimensions.

Combining all uncertainties quadratically produces a relative uncertainty value of:

$$Err_{\mathrm{tot}} \quad (3)$$

This the range of error, with a level of confidence of 95 %, is to be kept for further testing in order to adequately compare future results.

It is noted that this value is dominated by the pixel calibration error. Future campaigns should include fixed reference markers in the experimental setup to allow for a more precise calibration and significantly reduce this component of the uncertainty.

6. Conclusions

This study successfully developed and demonstrated a methodology for the rapid prototyping of satellite protection shields using 3D-printed carbon fibre and Kevlar composites. While the preliminary test campaign was primarily intended to validate this methodology and the associated analysis techniques, several important conclusions can be drawn from the ten hypervelocity impact tests performed.

The results indicate that manufacturing parameters, particularly printing orientation, have a significant effect on ballistic performance. Horizontally printed single plates appeared to be more efficient in resisting impact than vertically printed plates, which were prone to delamination and fracture between layers under high-energy impacts. This suggests that while horizontal printing is superior, further investigation is needed to overcome the technological constraints of using this orientation to build multi-plate Whipple-type shields, possibly by developing novel support or filler structures. The quantitative analysis procedures developed in Matlab™ for measuring damage and debris cloud characteristics proved to be effective indicators for determining the energy absorbed by the shields and comparing the efficiency of different geometries.

Horizontal production of simples appears to be more efficient than vertical production, however, it is necessary to understand how to overcome the technological constraint in order to use it to create whipple-type shields, investigating the possibility of constructing support or filler structures.

In addition, image analysis procedures developed on Matlab™ can be used as a quantitative indicator to determine the energy absorbed by the shields and evaluate the efficiency of the geometries tested.

The main limitations of this initial campaign were the small number of tests and minor production inconsistencies between samples. Furthermore, the use of a single high-speed camera limited the debris cloud analysis to two dimensions, necessitating some assumptions and simplifications. The adoption of a second camera would allow the cloud to be studied in three dimensions and possibly to avoid saturation problem at the moment of impact.

Finally, in a future test campaign, these structures will be compared to standard structures used to protect satellites with the same weight to determine the real improvement these structures bring to spacecraft shielding.

CRediT authorship contribution statement

Stefano Lopresti: Writing – original draft, Software, Methodology, Formal analysis, Conceptualization. **Leonardo Barilaro:** Writing – review & editing, Supervision, Resources, Funding acquisition. **Alberto Abiti:** Writing – review & editing, Software, Data curation. **Lorenzo Olivieri:** Writing – review & editing, Supervision.

Declaration of competing interest

The authors declare the following financial interests/personal relationships which may be considered as potential competing interests:

Leonardo Barilaro reports financial support was provided by Xjenza Malta. If there are other authors, they declare that they have no known competing financial interests or personal relationships that could have appeared to influence the work reported in this paper.

Acknowledgements

The work described in this paper is partially carried out as part of the SBORAEK (R&I-2022-002L) project which was financed by Xjenza Malta, through the FUSION–Technology Development Programme LITE. This activity has been performed in the framework of a collaboration between the Center of Space Studies CISAS “G. Colombo” of the University of Padova and the Malta College of Arts, Science, and Technology (MCAST).

The authors would like to thank Thiot Ingegnerie for the assistance in hypervelocity testing and to SkyUp Academy for the support.

References

[1] A.K. Nervold, J. Berk, J. Straub, A. Whalen, A pathway to small satellite market growth, Adv. Aerosp. Sci. Technol. (2016).

[2] F. Piergentili, N. Bellini, A. Locarini, S. Naldi, D. Rastelli, M. Valdatta, S. Bagassi, Fused deposition modeling techniques for manufacturing of cubesat based on modular design concept, in: 64th IAC, Beiking, China, 2013.

[3] L. Olivieri, C. Giacomuzzo, A. Francesconi, H. Stokes, A. Rossi, Experimental characterization of multi-layer 3D-printed shields for microsatellites, J. Space Safe. Eng. 7 (2) (2020) 125–136.

[4] B.N. Turner, S.A. Gold, A review of melt extrusion additive manufacturing processes: II. Materials, dimensional accuracy, and surface roughness, Rapid Prototyp. J. 21 (2015) 250–261.

[5] J.T. Belter, A. Dollar, Strengthening of 3D printed fused deposition manufactured parts using the fill compositing technique, PLoS One 10 (2015) 1–19.

[6] L. Li, Q. Sun, C. Bellehumeur, P. Gu, Composite modeling and analysis for fabrication of FDM prototypes with locally controlled properties, J. Manuf. Process. 4 (2) (2002) 129–141.

[7] ESA, Annual Space Environment Report, 2025.

[8] L. Olivieri, C. Giacomuzzo, F. Francesconi, Experimental characterization of multi-layer 3D printed shields for microsatellites, in: 69th IAC, 2018. Bremen, Germany.

[9] H. Hoshi, K. Nakano and Y. Iwahori, "Study on repair of CFRP laminates for aircraft structures," in *16th International Conference on Composite Materials*, Kyoto, Japan.

[10] R. Destefanis, E. Amerio, M. Briccarello, M. Belluco, M. Faraud, E. Tracino and C. Lobascio, "Space environment characterisation of kevlar®: good for bullets, debris and radiation too," Universal Journal of Aeroautical & Aerospace Sciences*,* pp. 80-113.

[11] A. Saleem, P.S. Ahmed, M.S. Abed, Experimental and numerical investigation of Kevlar and UHMWPE multi-layered armors against ballistic impact, Mater. Today 56 (2022) 2516–2524.

[12] R. Stevens, Concurrent engineering methods and models for satellite concept design, in: *IEEE Aerospace Conference*, Montana, USA, 2015.

[13] L.G. Blok, M.L. Longana, H. Yu, B.K.S. Woods, An investigation into 3D printing of fibre reinforced thermoplastic composites, Addit. Manuf. 22 (2018) 176–186.

[14] S. Harder, F. Röper, D. Gibhardt, B. Koert, B. Fiedler, Strength of scarf-bonded CFRP repairs containing disc-shaped zones of weak bonding considering hot-wet conditioning, Int. J. Adhesion Adhes. (2020) 102.

[15] M. Mao, Z. Meng, X. Huang, H. Zhu, L. Wang, X. Tian, J. He, D. Li, B. Lu, 3D printing in space: from mechanical structures to living tissues, Int. J. Extrem. Manuf. 6 (2) (2024).

[16] W. Wu, P. Geng, G. Li, D. Zhao, H. Zhang, J. Zhao, Influence of layer thickness and raster angle on the mechanical properties of 3D-printed PEEK and a comparative mechanical study between PEEK and ABS, Materials 8 (2015) 5834–5846.

[17] A. Rossi, Al, Rthe H2020 Redshift Project: a Successful European Effort Towards Space Debris Mitigation, 70th International Astronautical Congress, Washington D. C., USA, 2019.

[18] L. Barilaro, L. Olivieri, M. Wylie, S. Zaninotto, M. Baldissera, An overview on Smart Ballistic Optimization for Repairin of Aerospace Exostructures using 3D printed Kevlar, in: *74th IAC*, Baku, Azerbaijan, 2023.